Effect of transient solute loading on free convection in porous media

Yueqing Xie,[1,2] Craig T. Simmons,[1,2] Adrian D. Werner,[1,2] and James D. Ward[3]

Received 16 March 2010; revised 28 June 2010; accepted 12 July 2010; published 4 November 2010.

[1] Previous studies of free convection in porous media almost exclusively consider time-invariant solute boundary conditions and neglect the transient fluctuations that are inherent in natural systems. We study the effect of transient solute loading on the migration of dense salt plumes in an unstable setting using numerical simulations of a modified form of the classic solute analogue Elder problem. The numerical results show that for the periodic solute loading case, (1) a free convection slipstream (i.e., the downward movement of groundwater associated with a convection cell behind a descending salt blob) is observed such that newly developed successor fingers may be drawn toward the tails of convection cells associated with predecessor fingers; (2) the free convection slipstream intersects the top boundary layer, creating a boundary layer convective memory during solute loading-off periods in cases with periodicity less than some critical transitional convective periodicity (approximately 5 to 10 years for the current setting); and (3) the boundary layer convective memory causes newly developed successor fingers to form in the same locations and to migrate along the same pathways as their predecessor fingers (mutual dependence between successor and predecessor finger sets) and subsequently reinforce old fingers and enhance solute transport. Results from both quantitative diagnostics (e.g., Sherwood number, total mass of solute, vertical center of mass) and qualitative inspection clearly demonstrate that the periodicity of the solute-loading function controls the fingering process and the total solute transport behavior. Transient solute loading is more important in unstable free convection processes than has previously been recognized.

Citation: Xie, Y., C. T. Simmons, A. D. Werner, and J. D. Ward (2010), Effect of transient solute loading on free convection in porous media, *Water Resour. Res.*, *46*, W11511, doi:10.1029/2010WR009314.

1. Introduction

[2] The stratification of dense water overlying less dense water (i.e., due to salinity contrasts) can give rise to the occurrence of significant density gradients potentially leading to the development of gravity-driven instabilities. Under these circumstances, free convection of dense water and the associated generation of saline fingers can occur (i.e., the onset of instabilities), leading to enhanced solute transport which can accelerate the hydrodynamic mixing of different fluids within shorter time scales and over longer distances than that caused by diffusion alone. The reader is referred to comprehensive reviews by *Simmons et al.* [2001], *Simmons* [2005], and *Diersch and Kolditz* [2002] on this subject. Examples of naturally occurring free convection processes include groundwater salinization associated with transgressions [*Kooi et al.*, 2000], transport of accumulating salts near the land surface of a salt lake [*Wooding et al.*, 1997; *Simmons and Narayan*, 1997], and leakage from waste disposal sites [*Frind*, 1982; *Zhang and Schwartz*, 1995].

[3] Previous studies of free convection in groundwater almost exclusively consider time-invariant concentration boundary conditions and rarely incorporate the fluctuations that are inherent in natural systems (e.g., diurnal/seasonal/decadal variations in salinity). In general, they simply neglect the variability in solute loading by implicitly or explicitly assuming that the time scales of interest are considerably longer than the period of the salinity fluctuations [e.g., *Frind*, 1982; *Simmons and Narayan*, 1997; *Wooding et al.*, 1997; *Graf and Therrien*, 2007; *Post and Prommer*, 2007]. However, this assumption has not previously been systematically and quantitatively tested in relation to its effect on free convection in porous media.

[4] *Zhang and Schwartz* [1995] have reported that the nature of solute loading is one of the significant factors that impacts the development of plumes when examining the evolution of multispecies contaminant plumes under both intermittent and continuous source loadings. Several other examples have also demonstrated the potential importance of temporal solute loading, including the periodic dissolution of soluble minerals by recharging rainfall or seawater inundation in coastal sabkhas [*Butler*, 1969; *Wood et al.*, 2002], the climate-controlled filling and drying of closed desert

[1]School of the Environment, Flinders University, Adelaide, South Australia, Australia.
[2]National Centre for Groundwater Research and Training, Flinders University, Adelaide, South Australia, Australia.
[3]SA Water Centre for Water Management and Reuse, University of South Australia, Adelaide, South Australia, Australia.

0043-1397/10/2010WR009314

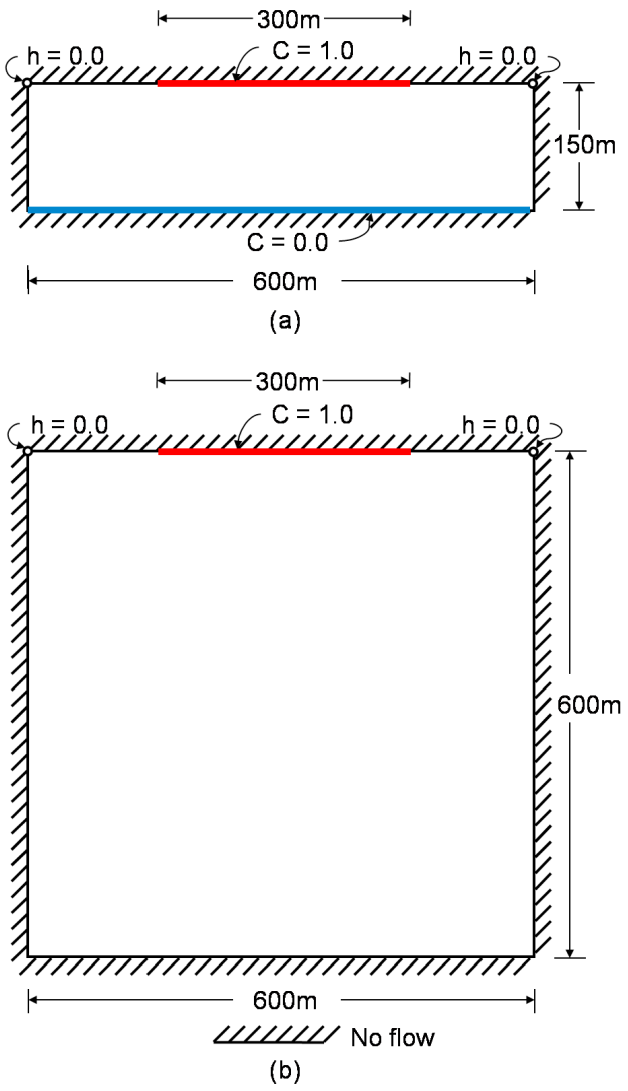

Figure 1. The model geometry for (a) classic Elder problem and (b) modified Elder problem. In the modified case, the bottom boundary condition is no solute flux, the vertical extent is increased from 150 m to 600 m, and the molecular diffusion coefficient is decreased from 3.565×10^{-6} m^2/s to 2.8×10^{-9} m^2/s while both longitudinal and transverse dispersivities are increased from 0.0 m to 1.0 m.

basins [*Fan et al.*, 1997], and the salinity fluctuations of tidal creeks [*Lenkopane et al.*, 2009]. However, none of these studies has explored the relationship between transient solute loading and free convection.

[5] Solute free convection has strong similarity to that of thermal free convection. By comparison, free convection with transient boundary conditions has been studied in heat transfer problems by heating the bottom both periodically and monotonically [*Nield and Bejan*, 2006, pp. 228–231]. *Chhuon and Caltagirone* [1979] found that lower-frequency transient heating plays a more important role in thermal free convection development than higher-frequency transient heating. How important the effect of transient boundary behavior is on solute free convection still requires quantitative evaluation.

[6] Recently, the role of spatial heterogeneity on free convection has been studied to understand the effect of complexity in geological formations on the onset, growth, and decay of solute plumes [e.g., *Schincariol and Schwartz*, 1990; *Simmons et al.*, 2001; *Prasad and Simmons*, 2003]. How the time-dependent solute loading influences the solute behavior still remains uncertain, and what the consequences of steady state simplifications of transient unstable systems are also remains unclear. Indeed, temporal solute loading is expected to play a very significant role in the behavior of density-dependent systems [*Simmons*, 2005].

[7] In this study, we carry out the first systematic investigation of free convection processes in the presence of periodic solute loading. The finite element subsurface groundwater flow model FEFLOW [*Diersch*, 2005] was employed to simulate the groundwater flow and solute transport responses to cyclic salinity loadings. The main objective of this study was to compare and contrast plume behavior under periodic and constant solute boundary conditions and to therefore assess the importance of periodicity in solute loading on free convection processes.

[8] The classic solute analogue Elder problem [*Elder*, 1967; *Voss and Souza*, 1987], a widely accepted and studied example of free convection phenomena, is modified to serve as the basis for the analyses of periodic solute loading. Solute periodicity is represented in numerical experiments as sequences of solute-on-solute-off conditions, imposed at the top boundary. Several measurable diagnostics, including those adopted by *Prasad and Simmons* [2003, 2005], are used to quantify the characteristics of modeling results, rather than relying on visual inspection alone. These include the Sherwood number, total mass of solute, center of gravity, the number of fingers, and the number of blobs. The results of this study provide initial insight into the influence and importance of natural transient fluctuations in boundary conditions on free convective transport.

2. Elder Problem

2.1. Classic Elder Problem

[9] The Elder problem is a widely accepted and studied example of free convection phenomena, in which fluid density differences drive the movement of fluids. It was established by *Elder* [1967] as both laboratory and numerical experiments which were aimed at producing thermal convection in a porous layer. *Voss and Souza* [1987] then transformed the thermal Elder problem into a solute analogue convective problem by enlarging the geometry and imposing a salt-water boundary condition at the top (hereafter we refer to the *Voss and Souza* [1987] version as the "classic Elder problem"). *Voss and Souza* [1987] utilized the classic Elder problem to benchmark the SUTRA code, a numerical simulator of density-dependent groundwater flow and solute transport, by comparing the salt contours with heat contours from the thermal Elder problem. Since then it has been widely used by numerous authors [e.g., *Oldenburg and Pruess*, 1995; *Kolditz et al.*, 1998; *Ackerer et al.*, 1999; *Diersch and Kolditz*, 2002] to test numerical simulators of variable density groundwater flow and solute transport.

[10] Figure 1a illustrates the classic Elder problem, in which a constant solute source with a unit relative concentration ($C = 1.0$) is placed along the middle half (300 m) of the top boundary to act as a constant concentration boundary

Table 1. Simulation Parameters for Both the Classic and the Modified Elder Problem

Parameter	Symbol	Classic	Modified	Unit
		Model Domain/Grid Size		
Model length	x	600	600[a]	m
Model height	y	150	600	m
Element length	Δx	3.4	3.4[a]	m
Element height	Δy	1.5	0.75 ($0 < y < 50$ m); 1.5 ($50 < y < 600$ m)	m
		Aquifer and Fluid Properties		
Permeability	k	4.845×10^{-13}	4.845×10^{-13}[a]	m^2
Effective porosity	ε	0.1	0.1[a]	-
Longitudinal dispersivity	β_L	0.0	1.0	m
Transverse dispersivity	β_T	0.0	1.0	m
Molecular diffusion coefficient	D_d	3.565×10^{-6}	2.8×10^{-9}	$m^2\ s^{-1}$
Dynamic viscosity	μ	1.0×10^{-3}	1.0×10^{-3}[a]	$kg\ m^{-1}\ s^{-1}$
Freshwater density	ρ_0	1000	1000[a]	$kg\ m^{-3}$
Gravitational acceleration	g	9.81	9.81[a]	$m\ s^{-2}$
Density contrast ratio	$\overline{\alpha}$	0.2	0.2[a]	-
Specific storage	S_s	1.0×10^{-4}	1.0×10^{-4}[a]	m^{-1}
		Initial and Boundary Conditions		
Initial freshwater head throughout	$h_{initial}$	0	0[a]	m
Initial concentration throughout	$C_{initial}$	0.0	0.0[a]	-
Scaled concentration at the top boundary	C_{top}	1.0	1.0 (when loading on);/(when loading off)	-
Scaled concentration at the bottom boundary	C_{bottom}	0.0	/	-
Head at upper corner nodes	h	0	0[a]	m

[a]Parameters are kept unchanged from the classic case. A forward slash in the table indicates that a boundary condition of no solute flux is applied.

condition. A zero concentration value ($C = 0.0$) is applied to the entire bottom boundary corresponding to the constant temperature boundary conditions of the thermal case. This allows solute to diffuse out of the system. No-fluid-flux boundary conditions on all sides restrict fluid flows to minor losses through the specified head nodes at the upper corner nodes. The initial conditions for the system are hydrostatic head and pure freshwater throughout. The maximum concentration of overlying dense water is 1200 kg/m^3, which is approximately equivalent to a salinity of 360,000 mg/L at standard conditions of atmospheric pressure and 25°C [*Adams and Bachu*, 2002]. This high value of concentration employed in the solute Elder problem is not atypical of salinities which may be encountered in a salt lake field setting [e.g., *Van Dam et al.*, 2009].

[11] The classic Elder problem employs a homogeneous and isotropic medium, and the dynamic viscosity is assumed to be independent of salt concentration. It should be noted that the diffusion coefficient value is representative of a thermal diffusion coefficient (3.565×10^{-6} m^2/s) but is still utilized as the solute diffusion coefficient for solute transport models in order to compare the corresponding results with Elder's original thermal results. In the early stages of the classic Elder problem, solute enters the regime by diffusion only (no convection) to form a boundary layer beneath the source zone. After sufficient solute accumulates within the boundary layer, instability fingers develop and gravitational processes start to drive the movement of fluids. The dimensionless Rayleigh number Ra is an indicator of the onset of instabilities in this system and is given by

$$Ra = \frac{k\rho_0 g\overline{\alpha}H}{\mu\varepsilon D_d} \tag{1}$$

where k is intrinsic permeability [L^2], g is acceleration due to gravity [LT^{-2}], $\overline{\alpha} = (\rho - \rho_0)/\rho_0$ is the density contrast coefficient [−], ρ_0 is freshwater density [ML^{-3}], ρ is saltwater density [ML^{-3}], H is the vertical extent of the flow regime [L], μ is dynamic viscosity [ML^{-1}T^{-1}], ε is effective porosity [−], and D_d is the aqueous molecular diffusion coefficient [L^{2}T^{-1}]. In comparison to the critical Ra of $4\pi^2$ in the Horton-Rogers-Lapwood problem with the infinitely extending horizontal porous layer and constant temperature at upper and lower boundaries [*Horton and Rogers*, 1945; *Lapwood*, 1948], the critical Ra in the classic Elder problem is zero because of the established concentration gradient at both outer edges of the boundary layer which cannot be removed by diffusion and which therefore must result in fluid flow [*van Reeuwijk et al.*, 2009]. Both the original and classic Elder problems are characterized by $Ra = 400$ [*Elder*, 1967; *Voss and Souza*, 1987], much greater than the critical value, and therefore free convection processes dominate salt transport following the development of the boundary layer. All the parameters for the classic Elder problem are listed in Table 1. The solute distribution in the classic Elder problem after 20 years is shown in Figure 2a. In the current study, we modify the classic Elder problem (as described in the following subsections) so that free convection processes under transient solute loading scenarios can be better evaluated. The reasons for these modifications are outlined in subsequent sections.

2.2. Modified Elder Problem

2.2.1. Solute Dispersion

[12] In free convection situations, diffusion and dispersion act to "dissipate" salt fingers by reducing density gradients within the interface between solute plumes and the ambient groundwater. The molecular diffusion coefficient (D_d) of 3.565×10^{-6} m^2/s used in the classic Elder problem is the thermal diffusivity and is three orders of magnitude higher than typical values of the molecular diffusion coefficient used in solute transport problems. The high value of D_d produces

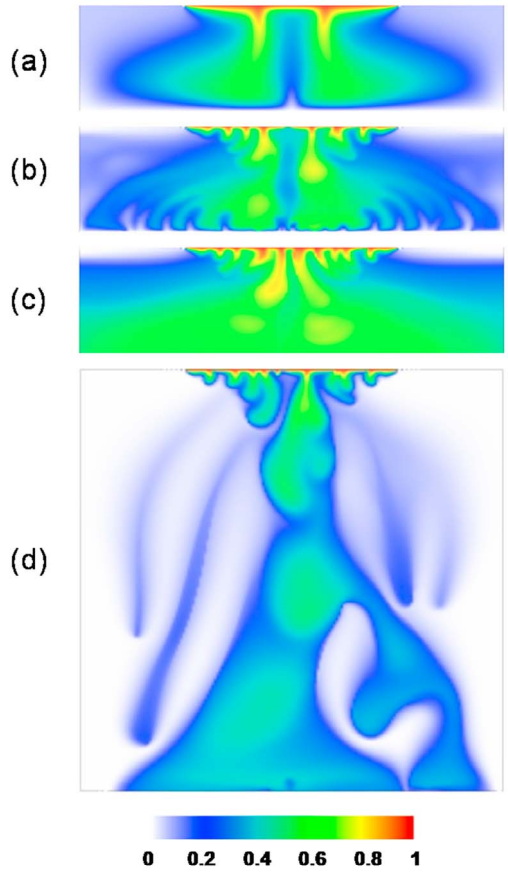

Figure 2. Salt distributions after 20 years showing the progressive modifications of the classic Elder problem into the modified Elder problem used in this study from (a) the classic Elder problem; (b) same as Figure 2a except with a molecular diffusion coefficient of 2.8×10^{-9} m^2/s and both longitudinal and transverse dispersivities of 1.0 m; (c) same as Figure 2b except the bottom concentration boundary condition is replaced by a no solute flux condition; and (d) same as Figure 2c except the vertical extent is increased to 600 m.

diffusive, symmetrical, lobe-shaped plumes, as illustrated in Figure 2a. Velocity-dependent mechanical dispersion (D_β), caused by the variability in pore sizes, path lengths, and pore frictions and commonly included in salt transport problems [e.g., *Abarca et al.*, 2007], is neglected in the classic Elder problem, and molecular diffusion plays an exclusive role in dissipating solute driven by concentration gradients.

[13] In the current study, D_d is decreased to 2.8×10^{-9} m^2/s (following *Simmons and Narayan* [1997]) to much better reflect the physics of salt transport. Mechanical dispersion D_β is introduced because of its dominance over molecular diffusion in the majority of solute transport problems involving real geological media [*Bear*, 1972, pp. 579–582]. D_β depends on longitudinal dispersivity (β_L) which transports solute in the direction of fluid flow, and transverse dispersivity (β_T) which spreads solute perpendicular to the fluid flow direction. *Schulze-Makuch* [2005] suggested that β_L increases exponentially with the length scale, on the basis of a compilation of data sets from laboratory experiments, aquifer tests, and modeling results. Using the empirical relationship of *Schulze-Makuch* [2005], a value of β_L of 1 m is used in accordance with the experimental length scale of 600 m (Figure 1). β_T is also specified as 1 m, identical to β_L (as per *Prasad and Simmons* [2003]) in order to simplify the current study to the simplest geologic situation although we are aware that it is slightly unrealistic. Importantly, the introduction of anisotropic dispersion is not expected to change the key results of the study.

[14] Gravity-driven fingers can be triggered by physically or numerically induced perturbations of density [*Diersch and Kolditz*, 2002]. Insufficiently fine grid discretization is an important numerical factor that causes perturbations because of improperly resolved concentration and/or hydraulic gradients. In the current study, the grid is designed to produce a Peclet number (*Pe*) that minimizes perturbations from inadequate mesh elements (i.e., $Pe < 4$; *Voss and Souza* [1987]). *Pe* is a ratio of convective transport to dispersive/diffusive transport and is given by [*Voss and Souza*, 1987]

$$Pe = \frac{|v|\Delta x}{D_d + |v|\beta_L} \approx \frac{\Delta x}{\beta_L} \tag{2}$$

where $|v|$ is the magnitude of local velocity [LT^{-1}], Δx is the characteristic elemental length along the flow direction [L], and β_L is the longitudinal dispersivity [L]. In most real aquifer cases, D_d is much lower than D_β and therefore D_d is typically neglected in defining *Pe* (as per equation (2)). Therefore, grid discretization should meet the requirement of $\Delta x < 4\beta_L$ [*Voss and Souza*, 1987]. In the current study, rectangular cells are used, and the discretization comprises $\Delta x = 3.4$ m horizontally and $\Delta y = 0.75$ m ($0 < y < 50$ m) and $\Delta y = 1.5$ m ($y > 50$ m) vertically. This discretization scheme produces 17,877 nodes, 17,600 elements, and a maximum *Pe* of 3.4 for the model domain shown in Figure 1a. The model domain of the final version of the modified Elder problem we arrive at in section 2.4 (Figure 1b) is represented using the same discretization scheme, producing 70,977 nodes and 70,400 elements. An adaptive time-stepping technique of forward Adams-Bashforth/backward trapezoid [*Diersch*, 2005] is applied with an initial time step of 0.001 day. A time step limit of 3 days was chosen to limit time step truncation errors. This value was obtained through repeated trial and error in the most severely fluctuating (smallest period) solute loading case in section 3. The highest value of time step limit that achieved numerical convergence was adopted throughout this study. The salt plume produced using D_β dispersion is illustrated in Figure 2b.

2.2.2. Bottom Concentration Boundary Condition

[15] The constant concentration ($C = 0$) condition at the bottom boundary of the classic Elder problem produces low-salinity fingers that rise because of buoyancy effects (Figure 2b). This occurs because solute is lost through diffusion across the bottom boundary from the model whereas water is retained because of the no-flow boundary condition. This creates an unstable buoyancy stratification in the vicinity of the bottom boundary condition. The resulting low-salinity groundwater moves upward under the combined effects of buoyancy and convective circulation, thereby influencing the downward movement of dense plumes. The corresponding constant temperature ($T = 0$) condition, in the original heat version of the Elder problem [*Elder*, 1967], was sensible because of the likelihood of heat losses out of this boundary of

Table 2. List of Numerical Experiments for Solute Cycle Periods

Case	Definition[a]
T_{const}	Constant concentration
$T_{0.1}$	(0.1 year, 0.1 year)
$T_{0.2}$	(0.2 year, 0.2 year)
$T_{0.5}$	(0.5 year, 0.5 year)
T_1	(1 year, 1 year)
T_2	(2 years, 2 years)
T_5	(5 years, 5 years)
T_{10}	(10 years, 10 years)
T_{50}	(50 years, 50 years)

[a]Times indicated in brackets are (solute loading on T_{on}, solute loading off T_{off}).

the model. However, it does not make sense in a solute version of the Elder problem. It is extremely unlikely that this phenomenon (i.e., removal of salts and subsequent generation of low-salinity fingers) would occur in natural systems since this bottom $C = 0$ boundary condition is not physically realistic in a solute analogue. Therefore, the bottom $C = 0$ boundary condition of the classic Elder problem is completely replaced by a default no-solute-flux boundary condition, in an identical fashion to that used by *Post and Prommer* [2007] in their Elder problem analysis. This eliminates buoyant low-salinity fingers from being generated at this bottom boundary, as shown in Figure 2c.

2.2.3. Geometry and Time Scale

[16] The vertical extent of the classic Elder problem is increased from 150 m to 600 m to allow for more room for development of descending fingers and blobs. The time for dense salt plumes to reach the bottom of the model therefore increases from approximately 4 years in the classic case to 17 years in the modified case. The overall time scale of the simulations are correspondingly increased to 100 years to more than compensate for the increased time it would take for fingers to transcend the larger vertical domain and subsequently occupy the porous box. Most importantly, this time scale allows us to introduce multiple cycles of descending plumes to during the simulation. Figure 2d illustrates the resulting dense plume in the enlarged regime after 20 years. This result shows the final modified Elder problem. The parameters used in this modified Elder problem are listed in Table 1 along with those used in the classic Elder problem.

2.2.4. Characteristics of the Modified Elder Problem

[17] The modifications made to the classic Elder problem as described above result in an extremely high *Ra* of nearly 2×10^6, compared to $Ra = 400$ for the classic Elder problem. This *Ra* indicates an oscillatory convection regime in which the creation and disappearance of unstable convection cells will continuously occur. The highly unstable behavior is clearly evidenced by a larger number of fingers propagating from the boundary layer (compare Figures 2a and 2d). Moreover, as pointed out by *Mazzia et al.* [2001] in their analysis of numerical reliability of the salt lake problem, grid convergence for this type of highly unstable plume behavior will not be achieved and should not be expected even with very fine discretization due to the strongly unstable characteristic of the convection regime.

[18] Interestingly, previous studies have not reported on the "natural equivalence" of the Elder problem when considering the density difference employed in that problem and how that might relate to natural groundwater problems. The extremely high salinity of 360,000 mg/L represented by the top boundary condition makes the problem relevant to natural salt lake settings. A recent study carried out by *Van Dam et al.* [2009] to detect saline fingers in a sabkha (salt lake) setting identified that the overlying dense water can have salinities of about 394,000 mg/L. By reducing the high diffusion and introduced dispersivities, the modified Elder problem can be assumed to be a better representation of salt lake problems. The transient phenomena reported in this paper, however, are also expected to be applicable over a wider range of Rayleigh numbers and at lower-density contrasts.

3. Periodic Solute Loadings

3.1. Conceptual Model

[19] The top concentration boundary condition is modified to simulate various periodic solute-on-solute-off sequences, which are intended to represent different solute loading patterns in an idealized manner. During solute-on periods, solute enters the system from the source zone (i.e., $C = 1.0$ boundary condition), whereas during solute-off periods no solute enters the system across the boundary (i.e., there is no C boundary condition). The duration of solute-on is termed "time on" (T_{on}), and the solute-off duration is referred to as "time off" (T_{off}). Each cycle of solute-on-solute-off is intended to induce sequences of solute influx followed by plume redistribution, and the nature of this behavior is tested using various cycle periods (i.e., $T_{on} + T_{off}$). Eight different periodic solute loading cases are reported here, ranging from high frequency, i.e., (T_{on}, T_{off}) = (0.1 year, 0.1 year), to a single cycle, i.e., (T_{on}, T_{off}) = (50 years, 50 years), as listed in Table 2. All simulations involve a total duration of 100 years and only cases where $T_{on} = T_{off}$ are considered. Therefore, all periodic loading cases have the same total T_{on}, i.e., the same "total solute receptive opportunity" of 50 years. This is an important design feature in this study.

3.2. Qualitative Observations

[20] Figure 3 illustrates the plume patterns from cases T_{const}, $T_{0.1}$, T_1, T_5, T_{10}, and T_{50}. The influence of solute periodicity was ascertained by comparing simulations of cyclic solute boundary conditions to the constant boundary concentration case (case T_{const}; Figure 3a). Even with constant solute loading, free convection processes in the modified Elder problem setting are markedly different to previous adaptations of the Elder problem. In the case T_{const}, a large number (i.e., relative to the classic Elder problem) of unstable fingers occurred during the initial stage. The corresponding short finger wavelength is expected given the high *Ra* for this situation [*Riaz et al.*, 2006]. The fingers coalesce as they descend to form large-scale salinity structures in the lower part of the domain. Finger descent induces groundwater flow circulations (i.e., vortices) that act to move freshwater upward, creating upwelling freshwater zones. Groundwater flow circulations were observed at both local (on the order of meters) and aquifer (on the order of hundreds of meters) scales. Local-scale circulations, occurring around individual fingers, influenced the interaction and coalescence between fingers. In comparison, aquifer-scale circulations, in which freshwater flows first upward near the vertical boundaries and then horizontally near the top boundary, forced fingers situated immediately beneath the boundary layer at both sides

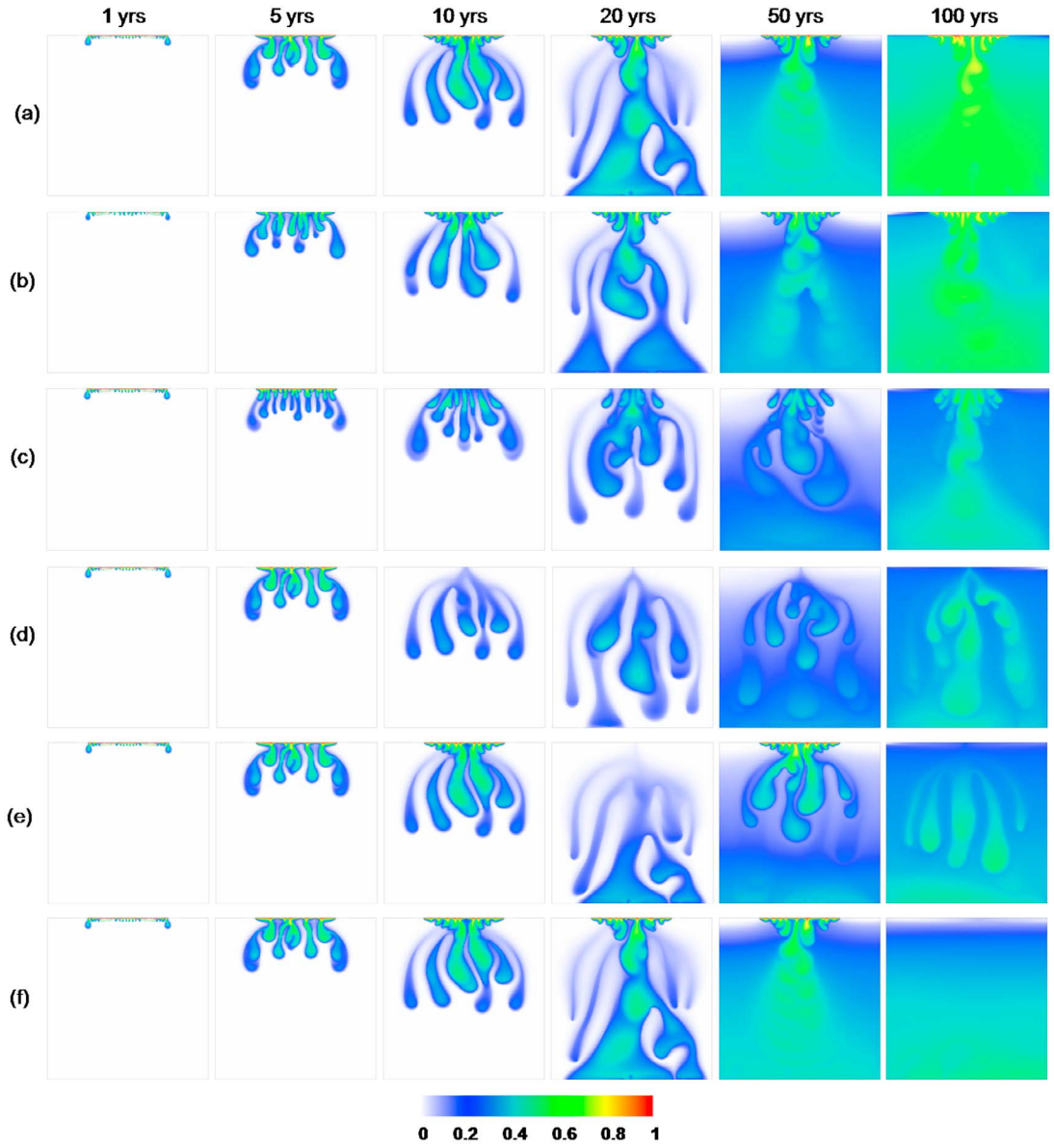

Figure 3. Salt plume distributions of (a) case T_{const}, (b) case $T_{0.1}$, (c) case T_1, (d) case T_5, (e) case T_{10}, and (f) case T_{50} at the simulation times of 1, 5, 10, 20, 50, and 100 years, respectively.

to centralize. These fingers grow by capturing smaller fingers when migrating toward the center as can also be seen in the salt lake problem [*Simmons et al.*, 1999]. As a consequence, fingers generated from the upper boundary layer were "funneled" into voluminous saline plumes in the center region of the domain. Once the plume reached the bottom of the domain, salt accumulated in the lower part of the domain and gradually increased the concentration of the ambient groundwater in the system. This in turn caused convection to progressively weaken because of the reduced density gradient between saline fingers and ambient groundwater.

[21] Changing the top boundary from constant to periodic concentration conditions resulted in significant changes to convection processes and the resulting transport of saline groundwater fingers, as shown in Figures 3b, 3c, 3d, 3e, and 3f). For example, under certain conditions saline fingers detach from the top boundary to produce saline blobs; the extent of detachment appears to depend on T_{off} of different loading cases. In case $T_{0.1}$ (Figure 3b), the fingers remain connected to the top boundary and receive solute influx via residual saline groundwater pathways that persist within the boundary layer during T_{off} periods. In case T_{50} (Figure 3f), fingers eventually disappear from the system through dispersive mixing and the extended period without solute supply. In intermediate situations, disconnection ranges from partial detachment (e.g., case T_1, Figure 3c) to complete detachment (e.g., case T_{10}, Figure 3e). These results suggest that there is a characteristic "critical transitional convective periodicity," which is the minimum time scale that produces complete disconnection of saline fingers and where successor and predecessor fingers become mutually exclusive for larger periods. Case T_5 (Figure 3d) results in only one saline

finger remaining attached to the top boundary, and therefore the critical transitional convective periodicity is on the order of 5 to 10 years in the current setting. This value is approximate only and is clearly specific to the adopted hydrogeologic parameters: additional simulations would be required to produce a generalized value. Our intention here is not to produce a generalized result, but rather to illustrate this phenomenon.

[22] The periodicity of the solute simulations produced novel insight into finger formation processes. For example, newly developed fingers (i.e., generated at the start of each new T_{on} phase) tend to migrate toward the pathways of previously formed fingers. This is best demonstrated in case T_1 (Figure 3c, at 5 years), case T_5 (Figure 3d, at 20 years), and case T_{10} (Figure 3e, at 50 years), in which new fingers follow the routes of old, dispersed fingers. This phenomenon is induced by remnant groundwater circulations associated with sinking fingers or detached blobs (i.e., local-scale vortices), which persist during T_{off} phases and clearly drive new fingers to migrate in precisely the same direction and locations of previous finger descent pathways. In general terms, we expect that the influence of existing fingers on the routes of new ones depends on the strength of convective vortices. We coin this previously undocumented phenomenon the "free convection slipstream," through which new fingers change their descent pathways to follow previously formed fingers.

[23] When the convective vortices of existing fingers intersect the boundary layer during the T_{off} phase, new fingers developing at the boundary layer in the following T_{on} phase are preferentially funneled into the slipstream, and these fingers tend to form in the same location as predecessor fingers (i.e., successor/predecessor sets of fingers are therefore not mutually exclusive but are rather mutually dependent). We refer to this newly observed phenomenon as the "boundary layer convective memory" at the end of T_{off} period. When T_{off} is sufficiently large, the location and strength of the convective vortices is such that they no longer intersect the boundary (i.e., there is no boundary layer convective memory). New fingers thus form in positions that are mutually exclusive and unrelated to predecessor finger sets. The qualitative observations described here are analyzed using quantitative measures in the following subsections.

3.3. Quantitative Analysis

[24] The numerical experiments have been visually inspected above by examining the concentration distributions. Those qualitative results show that imposing the periodic solute loading on the base case makes the system more transient and complicated. Evidently, rigorous quantitative analysis is required in order to make systematic and objective comparisons.

[25] *Prasad and Simmons* [2003] proposed measurable quantities for characterizing unstable flow situations as an improvement over simple visual inspection. They used the Nusselt number, the total amount of solute in the aquifer, and plume center of gravity in their analysis of heterogeneity effects on variable density transport. The following diagnostics are used to characterize convective processes occurring in the numerical experiments of the current study (following similar approaches by *Prasad and Simmons*, 2003, 2005): (1) Sherwood number (*Sh*), (2) total mass of solute (TM), (3) solute plume center of gravity (COG), (4) number of fingers (NOF), and (5) number of blobs (NOB).

[26] The dimensionless Sherwood number [*Nield and Bejan*, 2006, pp. 376–377], the solute analogue to the (thermal) Nusselt number used by *Prasad and Simmons* [2003], is the ratio of the rate of actual mass transfer due to free convection during the transient state to the rate of mass transfer due to diffusion, and is given by

$$Sh = \frac{mH}{WL_s D_d \Delta C} \tag{3}$$

where m is the mass flux across the source boundary [L^3T^{-1}], W is the width of the source zone, and is equal to unity for the cross-sectional layout of the domain [L], L_s is the length scale of the source zone [L], and ΔC is the maximum concentration difference between freshwater and saltwater [−].

[27] TM is the total amount of solute mass transferred to and contained in the groundwater system during the simulation. COG is the vertical center of gravity of solute plume throughout the system measured from the top boundary and provides a diagnostic of the vertical salinity distribution as per *Prasad and Simmons* [2003]. NOF is the number of continuous fingers in the entire model that are attached to the top source boundary, whereas NOB is the number of discrete solute plumes or blobs also in the entire model (but disconnected from the source boundary), which are defined by regions bounded by a closed relative concentration (C) contour.

[28] Note that these are a mix of macroscopic variables (i.e., *Sh*, TM, and COG) and microscopic diagnostics (i.e., NOF and NOB) that identify particular features of the free convection process. We use the term "macroscopic" and "microscopic" to reflect large- and small-scale behavior respectively. The macroscopic variables are integrated over a certain space in every single time step, whereas microscopic diagnostics are manually counted on the basis of the specific criteria. Macroscopic diagnostics are expected to be less sensitive to grid discretization, adaptive time-stepping schemes, numerical solvers, etc., than microscopic ones because of their integrating effects. Macroscopic diagnostics can display general trends of overall plume behavior, while microscopic diagnostics highlight small-scale details. Comparing macroscopic and microscopic diagnostics in a quantitative way is critical in order to understand what aspects of this unstable system behavior are predictable.

3.3.1. Sherwood Number (*Sh*)

[29] Figure 4a shows the variation of Sherwood number in case T_{const}, in which small-scale *Sh* oscillations occur, in addition to larger-scale temporal trends. Five main stages are observed in this numerical experiment (i.e., A–F in Figure 4a). Initially (A–B), high-concentration gradients produce high *Sh* and lead to the formation of the boundary layer by means of diffusion under initially hydrostatic conditions. Instability fingers develop once the boundary layer is sufficiently thick, causing an increase in *Sh* (B–C). The descent of fingers subsequently produces aquifer-scale circulations, and the upwelling of freshwater funnels the fingers toward the center of the domain and acts to impede the boundary influx of salt, thereby reducing *Sh* (C–D). This is followed by a period of relative *Sh* equilibrium (D–E), whereby fingers continuously

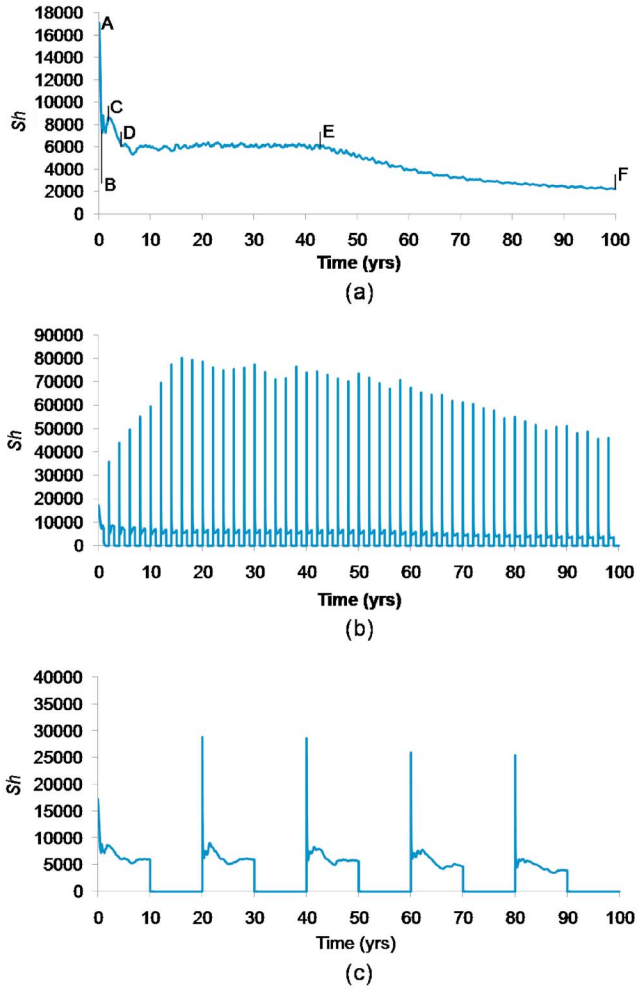

Figure 4. *Sh* versus time: (a) case T_{const}, (b) case T_1, and (c) case T_{10}.

migrate downward and pile up from the bottom. Note that the contact of the plume with the bottom boundary at 17 years does not appear to have instantaneous influence on the solute transfer. The continuing accumulation of solute in the aquifer eventually results in a reduced concentration gradient in the vicinity of the upper boundary, and thereby *Sh* gradually decreases (E–F).

[30] Figures 4b and 4c illustrate the *Sh* trends for two cases of periodic solute loading. The plots show regular spikes in *Sh* occurring immediately after the start of each cyclic loading period. Actually, at the very start of each loading period a numerical oscillation was observed in which *Sh* increased by many orders of magnitude, and then decreased to a negative value of the same order. These oscillations are caused at the sharp fronts of the very thin boundary layer, which is immediately established after the start of new loading, because of the extremely high *Ra*. They can be either resolved by much finer mesh, which requires an enhanced computational effort, or suppressed by numerical damping (e.g., via numerical up-winding techniques). After *Gresho and Lee* [1981], it was decided that these oscillations should not be damped as they may lead to greater insight into the numerical model. Fortunately, they were seen to take place only over extremely short durations (never more than two time steps, and only ever at the very start of each loading period). They are not expected to have a significant impact on *Sh* evolution, an integral quantity, and can be neglected rather than resorting to much finer grid size and heavy computation in order to resolve the sharp concentration transitions at the start of T_{on} phases.

[31] Neglecting the numerically oscillatory behavior, *Sh* peaks were observed to be more oscillatory and reach larger magnitudes in cases of smaller periodicity (comparing Figures 4b and 4c) due to the different extent of the effect of local-scale and aquifer-scale circulations. As seen in Figure 3, fingers in case T_{10} detached from the top concentration boundary at the end of a cyclic period, and, therefore, only the aquifer-scale circulation influenced the solute influx at the start of a new solute loading. In comparison, both the local-scale and aquifer-scale circulations affect the new solute transfer behavior to cause strong variation in case T_1. *Sh* decreases quickly to a normal range (less than 10,000; this range also occurs in all other cases), and they exhibit remarkably similar solute transport behavior, i.e., fluctuating for a while and then entering a plateau. In addition, *Sh* dropped to zero during T_{off} phases, as expected. A gradual decrease in *Sh* is observed in the cyclic cases because of the accumulation of salt in the aquifer as was observed in case T_{const}.

3.3.2. Total Mass of Solute (TM)

[32] TM trends for cases T_{const} to T_{50} are illustrated in Figure 5. In all cases, the rate of solute accumulation gradually reduces in time because of the buildup of salts within the aquifer, and TM increases asymptotically toward the theoretical maximum salt storage capacity of the porous medium at 36,000 (dimensionless). Case T_{const} produces the largest TM because of the constant solute loading, while it represents the early stage TM relationship for the first cycle of all periodic cases. T_{off} periods produce plateaus in the TM curves, as expected. TM trends in cases T_1, T_2, T_5, and T_{10} are comparable and arrive at a similar 100 year TM value that coincides with that of case T_{50}: a somewhat intuitive outcome given that all cases have the same cumulative T_{on} and T_{off} durations of 50 years. However, the TM trends of relatively short cyclic periods (i.e., cases $T_{0.1}$, $T_{0.2}$, and $T_{0.5}$) diverge from the TM cluster of longer period cases (the quantity of solute increased), more so for shorter cyclic periods. This behavior is attributed to the occurrence of free convection slipstreams, as described in section 3.2, which are seen to enhance solute inflow transport. Note that the minimum TM at 100 years is nearly half of the maximum one in this series. Importantly, the T_{const} case produces the largest of the total mass transported into the system, and this demonstrates that the assumption of constant concentration boundary conditions overpredicts the salt flux when compared to the real transient system.

[33] The influence of the free convection slipstream is explored in more detail through evaluation of the velocity vector fields as illustrated in Figure 6. At the aquifer scale, groundwater circulation patterns are evident, whereby downward velocity vectors occur within instability fingers and in finger "tails" (i.e., demonstrating the free convection slipstream), which are otherwise surrounded by upwelling less dense groundwater. As illustrated in Figure 6b, the free convection slipstream attracts descending fingers toward previous finger pathways. In Figure 6a, the free convection slipstreams are also evident at the upper boundary at the end

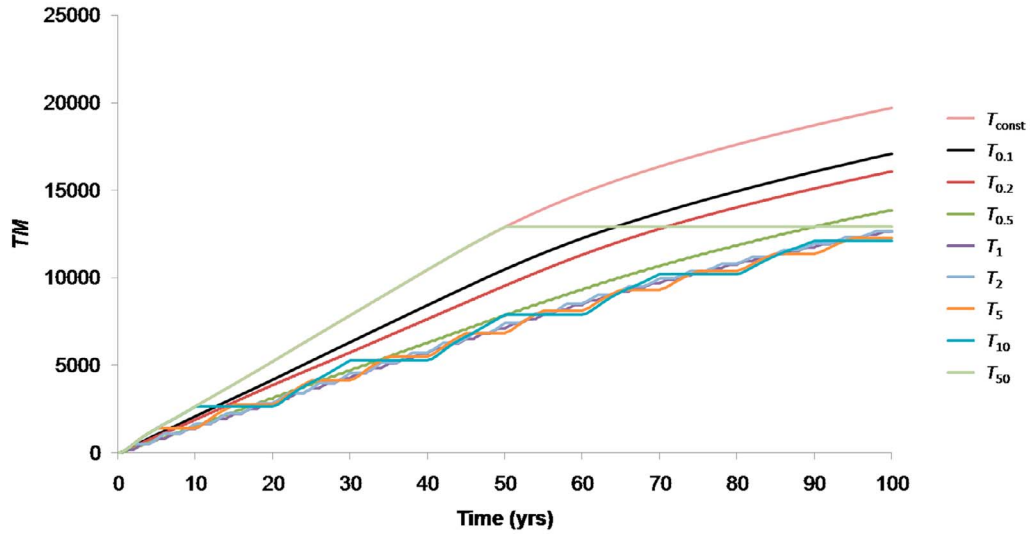

Figure 5. The comparison of variation in dimensionless TM versus time for values of source boundary condition periods.

of the T_{off} period (i.e., clearly defined velocity circulations associated with previous fingers) and are magnified in Figure 7a, displaying strong variation in velocity vectors. Figure 7b presents finger patterns and velocity vectors 10 days after the subsequent T_{on} period started. The results do not show obvious differences from those in Figure 7a apart from the reemergence of the $C = 1$ boundary condition represented by the red color at the top and the penetration of this new $C = 1$ condition into the old set of predecessor fingers. Clearly new fingers form rapidly at the same locations as their predecessor fingers because of the persistence of downward velocity vectors during the previous T_{off} phase, and new fingers (shown in red) are being funneled into the same pathways as their predecessors.

[34] An assessment of the vertical velocity distributions across the top boundary provides clear quantitative evidence of the boundary layer convective memory. Figure 8 shows the vertical velocity distribution at the upper boundary for cases $T_{0.1}$, T_1, T_5, T_{10}, and T_{50} after 100 years. The peaks in the downward velocity distribution (i.e., negative velocities) are consistent with instability fingers propagating from the top boundary (see Figure 3). The velocity magnitude is indicative of the strength of the free convection slipstream at the location of the upper boundary, decreasing with increasing period of solute cycling.

[35] Figure 9 illustrates the averaged magnitudes (AM) and standard deviations of vertical velocity vectors beneath the top concentration boundary after 100 years for all periodic

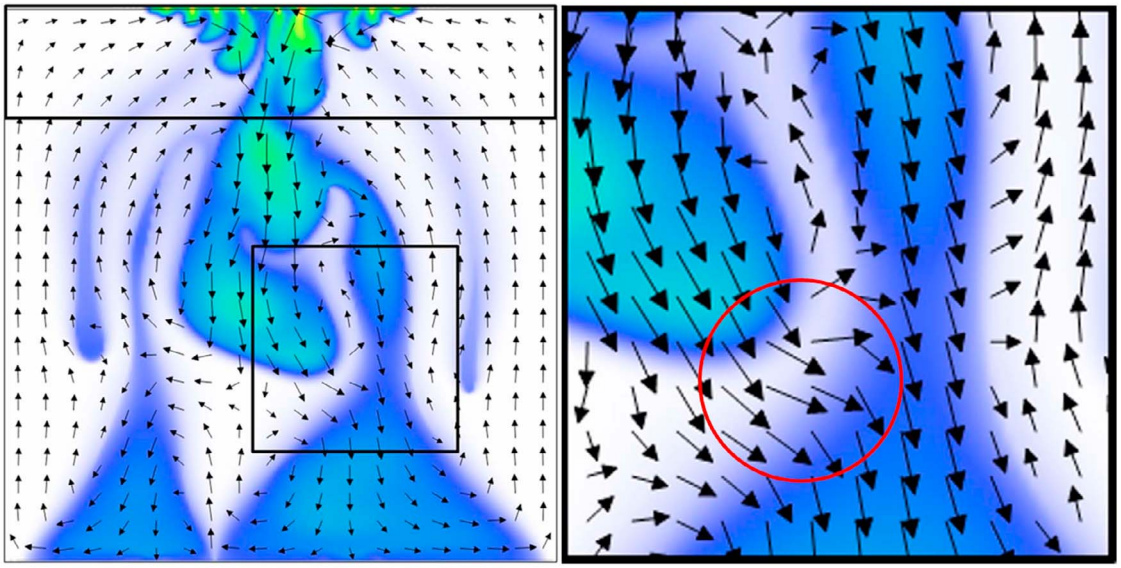

Figure 6. Velocity vector fields associated with finger patterns (a) in case $T_{0.1}$ after 20 years; (b) close-up of the square area in Figure 6a with the slipstream effect contained in the red circle.

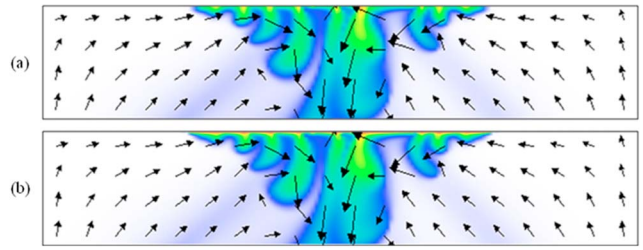

Figure 7. A close-up of velocity vectors along the upper boundary in case $T_{0.1}$ (the rectangular area in Figure 6a) at (a) 20 years when the system is about to receive solute and (b) 10 days after 20 years. A solute source has been reimposed onto the groundwater system (represented by the red color at the top representing $C = 1$), and fingers have already formed in exactly the same locations in Figure 7b because of the effect of boundary layer convective memory. This can be seen by the penetration of the new $C = 1$ (red) regions into the pathways of the older predecessor finger set shortly after the concentration boundary is turned back on.

loading cases. Very small AM and standard deviation in cases T_{10} and T_{50} indicate exceedingly weak and unnoticeable boundary layer convective memory due to long T_{off} values. The rapid increase in AM and standard deviation from case T_{10} to case T_5 marks the occurrence of boundary layer convective memory, which is consistent with the observation in section 3.2. The steady growth of AM and standard deviation from case T_5 to case T_2 indicates the increasing strength of the free convection slipstream. From case $T_{0.5}$ to $T_{0.1}$, the short period of solute cycling results in high standard deviation and AM, which indicates substantial free convection slipstream and explains the divergence of the associated TM curve from the cluster for these short periods of solute loading cases (Figure 5).

3.3.3. Solute Center of Gravity (COG)

[36] Temporal trends in COG (measured as a depth from the top of the domain) are shown in Figure 10. In case T_{const}, COG initially increases because of the descent of the first salt fingers, and then a reduced rate of COG increase occurs after the first fingers reach the bottom of the aquifer. COG reaches its peak of around 350 m at 28 years, and then declines and asymptotes to the vertical center (300 m) of the domain as the aquifer fills with solute.

[37] In cases $T_{0.1}$, T_1, and T_{10}, COG continuously descended (i.e., the curve rises) in the first entire injection cycle because of the initial absence of solute regardless of the injection patterns. Later, at the start of each T_{on} sequence, COG rises (i.e., the curve falls) because of the influx of salt near the top boundary. The magnitude of COG oscillations dissipate in time because of solute buildup, and the COG trends of periodic simulations start to mimic case T_{const} COG, i.e., asymptotically approaching the vertical center (300 m).

[38] The degree of fluctuation of COG grows with the increase in cyclic loading period. The COG curve in case $T_{0.1}$ differs slightly from that of the constant injection case, whereas in case T_{10} the COG strongly fluctuates. In addition, the time for intermediate cases (e.g., T_1) to reach the maximum COG is generally later than other short- and long-period cases (e.g., $T_{0.1}$ and T_{10}). In the constant and very short periodicity cases, the continuous fingering patterns are sustained by solute from the source, maintaining convective strength (compared with dispersive losses). Similarly, in the large period cases, although blobs are discontinuous, each blob involves substantial convective strength, and the larger mass of the blob means that dispersion is relatively less effective in dispersing the blob in any given time scale. In intermediate cases, blobs become disconnected, and their smaller size means that dispersion is relatively more effective at dissipating them.

3.3.4. Number of Fingers (NOF)

[39] NOF was defined to monitor the fingers that remain connected to upper source boundary in the whole domain. Figure 11 demonstrates the variation in NOF in cases T_{const}, $T_{0.1}$, T_1, and T_{10}, which was monitored once every 5 years after simulations started. Case T_{const} (Figure 11a) displays

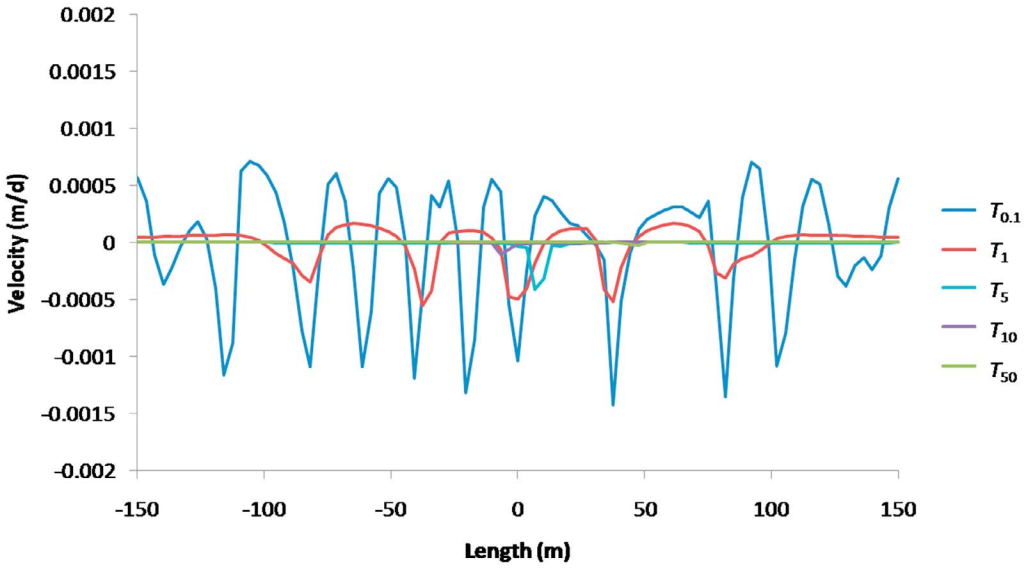

Figure 8. Vertical velocity distributions along the top source boundary in five cyclic loading cases after 100 years. Negative velocity values denote downward movement.

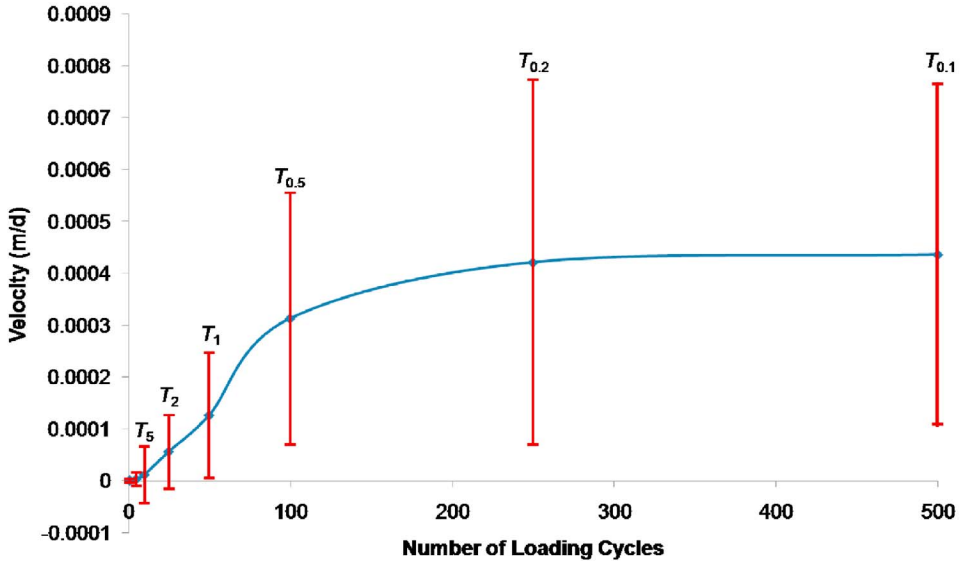

Figure 9. Averaged magnitudes of vertical velocity vectors along the top concentration boundary from case $T_{0.1}$ to case T_{50} after 100 years. Corresponding standard deviation of each case is plotted. The number of loading cycles is used in order to separate the cases with loading periods less than 1 year and provide better clarity on the details.

8 to 10 connected fingers at later times (from D onward in Figure 4a). Similarly, periodic loading cases tend to maintain a long-term NOF at around nine. Case $T_{0.1}$ (Figure 11b) behaves like case T_{const} because of the short period of solute cycling. A NOF spike of 18 at 5 years in case T_1 (Figure 11c) was caused by the weak aquifer-scale circulation along the top boundary during the first few years, and therefore fingers remained undisturbed compared to those at the same time in other cases (see Figure 3).

[40] NOF is seen to decrease with increasing period of solute cycling at the end of T_{off}. NOF decreases to about five at the end of T_{off} in case T_1, whereas NOF drops to zero in case T_{10}. This demonstrates clearly that the boundary layer convective memory decreases from case $T_{0.1}$ to case T_{50}. Clearly, NOF is very sensitive to the periodicity of solute loading.

3.3.5. Number of Blobs (NOB)

[41] Figure 12 shows the variation in NOB versus time in cases T_{const}, $T_{0.1}$, T_1, and T_{10}. NOB, defined using contours at 0.2 and 0.6 scaled concentrations and examined every 5 years after simulations commence, is used to quantify the extent of instability from the perspective of discrete blobs. The only trend for all the cases is the sudden rise of ($C = 0.2$) at very early times and the subsequent decrease to zero at later times because of the substantial accumulation of salt. In addition to this trend, significant variability can be seen with both NOB ($C = 0.2$) and NOB ($C = 0.6$) in all the cases including case T_{const}. There does not appear to be an obvious

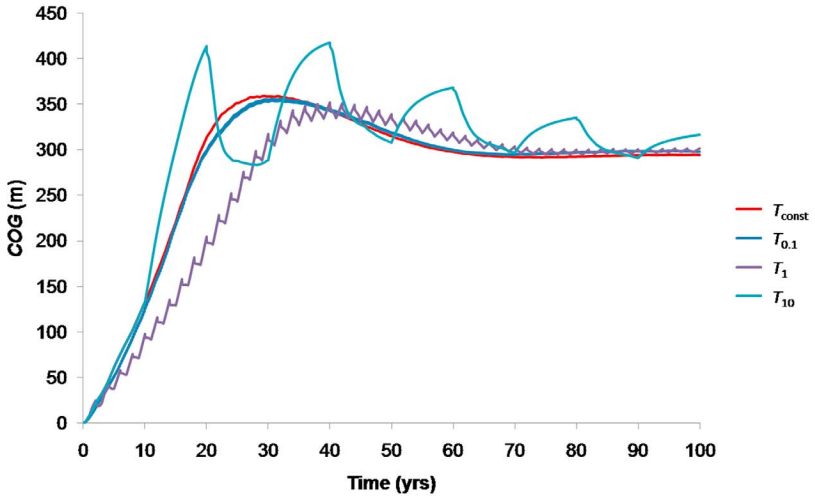

Figure 10. The temporal development of COG of solute plumes.

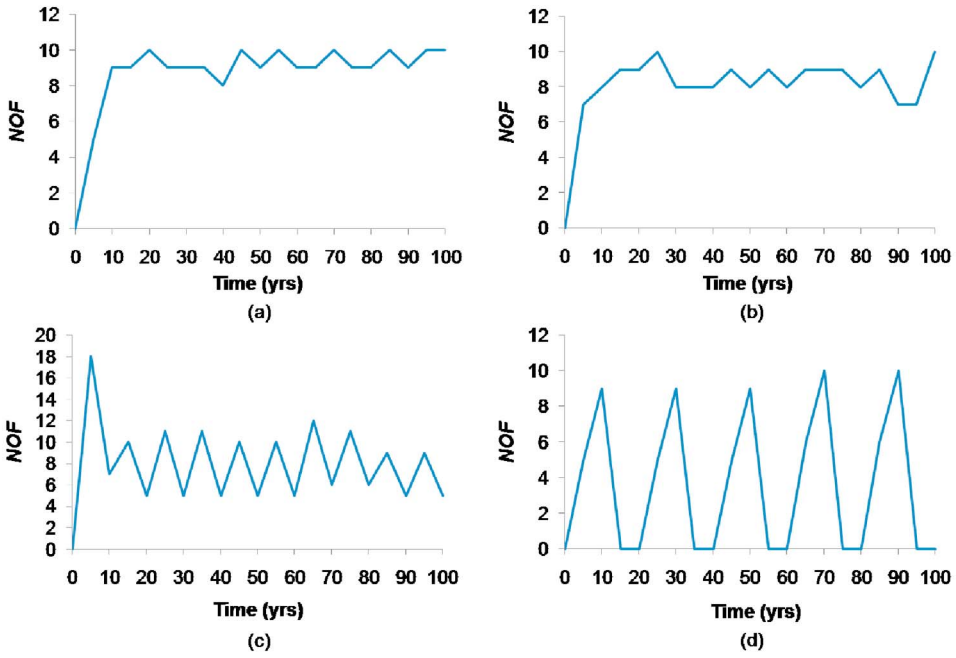

Figure 11. The variation in the number of fingers (NOF) versus time in (a) case T_{const}, (b) case $T_{0.1}$, (c) case T_1, and (d) case T_{10}.

relationship between NOB versus time functions and the boundary condition periodicity. Blobs occur because of the detachment of the fingers from the top boundary during loading-free periods, the quick accumulation of salt at the tips of some fingers, and the influence of strong convection of neighboring fingers which may induce a detachment by shearing local fingers away. Any combination of these physical processes can cause the variability in this microscopic diagnostic when quantifying the blobs. It should be noted that there are multiple solutions because of the lack of grid convergence as discussed in section 2.5, and therefore

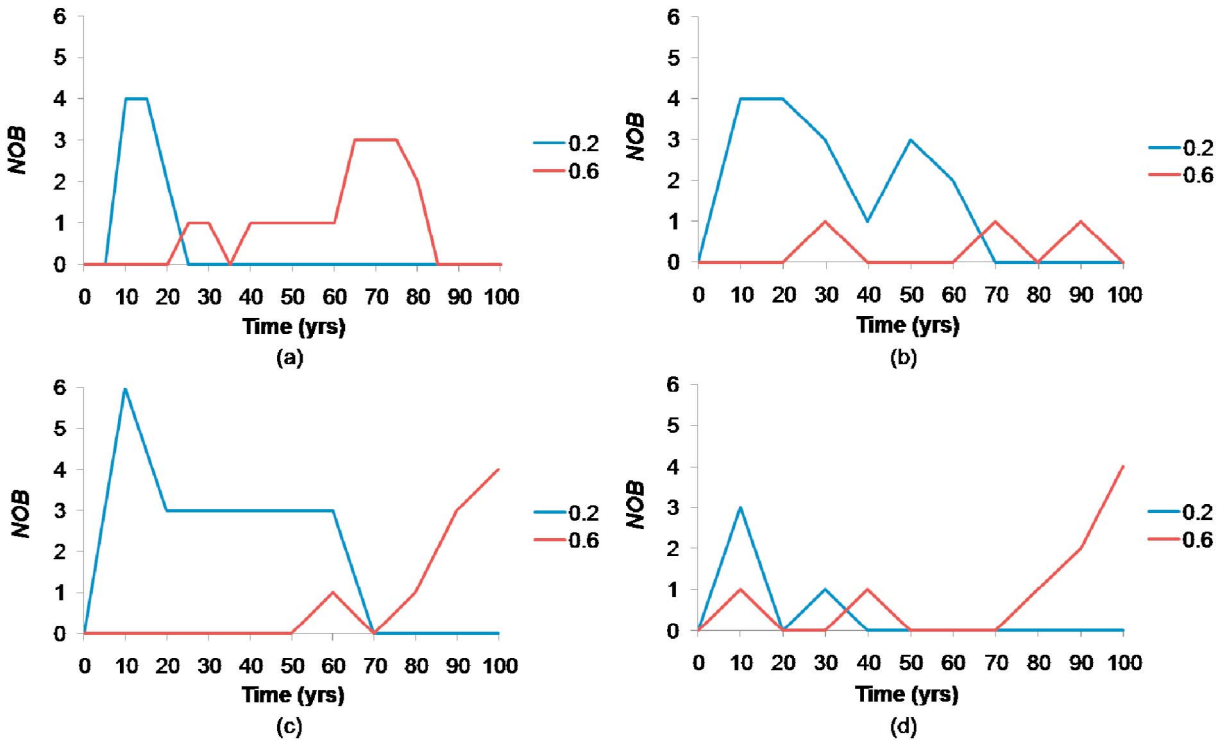

Figure 12. The variation in the number of blobs (NOB) bounded by a closed relative concentration contour for both $C = 0.2$ and $C = 0.6$ in (a) case T_{const}, (b) case $T_{0.1}$, (c) case T_1, and (d) case T_{10}.

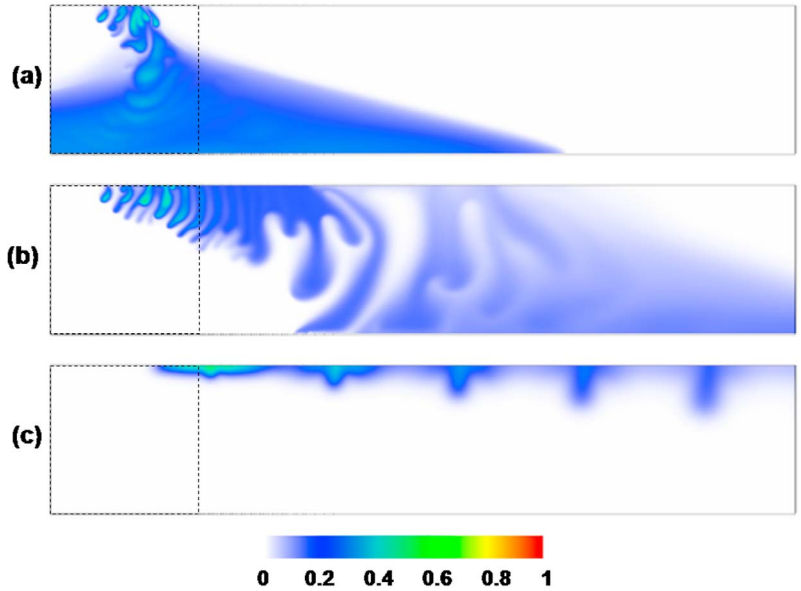

Figure 13. Salt distribution in the extended modeling domain in case T_1 under mixed convection: (a) $M_c = 120$, (b) $M_c = 12$, and (c) $M_c = 1.2$ after 100 years. Dashed line indicates original modeling domain.

this microscopic variable is not able to give deterministic answers but rather shows illustrative behavior.

3.4. Mixed Convection

[42] In the analyses described above, only free convection cases have been simulated and assessed. In the following trials, mixed convection is taken into consideration by including the influence of steady horizontal hydraulic gradient to examine the effect of periodic solute loading. The intention here is to explore transient solute loading in a more natural setting in which regional groundwater flow gradients exist. Hydraulic head boundaries are assigned along both vertical sides of the model, and these are used to create horizontal fluid flows across the aquifer. Mixed convection creates the possibility for salt to leave the model through the head boundary conditions applied in this "open" boundary case.

[43] Mixed convection is characterized by the mixed convection ratio M_c, which is the ratio of free convection driven by density gradient to the forced convection (advection) due to the applied external hydraulic gradient. The mixed convection ratio is given by

$$M_c = \frac{\left(\frac{\Delta\rho}{\rho_0}\right)}{\left(\frac{\Delta h}{\Delta L}\right)} \tag{4}$$

where $\Delta\rho$ is the density difference between saltwater and freshwater [ML^{-3}], Δh is the lateral hydraulic head difference across the flow regime [L], and ΔL is the length scale over which Δh is applied [L]. When $M_c \gg 1$, free convection dominates the regime; when $M_c \ll 1$, forced convection (i.e., advection) dominates; when $M_c \approx 1$, both free convection and forced convection are important and of comparable magnitude.

[44] Simulations were produced using M_c = 120, 12, and 1.2 (representing different degrees of mixed convection and typical hydraulic gradients found in natural systems) to inspect fingering processes in an intermediate cyclic solute loading case (i.e., case T_1). In the model, initial hydraulic head at the left-hand side boundary is specified as either 1 m, 10 m, or 100 m, respectively, along with 0 m at the right-hand side boundary to create the mixed convection ratios specified above. However, strong interaction between the plume and the lateral boundary conditions occurred in the strong advective case (e.g., M_c = 1.2). In order to minimize side boundary effects and maintain the mixed convection ratios, the lateral domain size was increased by 2400 m in the right-hand (downstream) direction to give a total lateral domain size of 3000 m. To maintain the head gradients and hence mixed convection ratios specified above, the hydraulic head at the right-hand side boundary is reduced to −4 m, −40 m, and −400 m for the three left-hand side boundary heads respectively.

[45] In all cases, the density difference was held constant; M_c was varied by changing the applied external head gradient. A hydraulic gradient of 1/600, which is the magnitude of a typical natural hydraulic gradient of 1/1000 [*Simmons*, 2005], gives M_c = 120, indicating stronger free convection and weaker forced convection. Meanwhile, with a hydraulic gradient of 1/6, which is reasonably unlikely to occur in nature and results in M_c = 1.2, was imposed on the aquifer in order to investigate cyclic solute loading under a more balanced mixed convection case, in order to test a more extreme "end member" scenario.

[46] Figure 13 illustrates the plume distributions at the end of the simulations at time 100 years for different mixed convection ratios in case T_1. The dashed square indicates the modeling domain of the base case we previously employed. Solute accumulated from the bottom first in the case of M_c = 120 (whole domain) although instability fingers were driven slightly to the right while penetrating the aquifer.

Solute then spreads along the bottom to both sides of the domain, which subsequently resulted in the discharge of solute from the left side boundary. Transported solute in the case of $M_c = 12$ was forced to move toward the right side boundary. However, the instability fingers still reached the bottom of the aquifer on their way to the right side boundary where solute eventually left the domain. The phenomenon of free convection slipstream and also boundary layer convective memory was still observed in both $M_c = 120$ and $M_c = 12$ cases (not shown here) if convection cells were retained along the source boundary when new solute loading was about to take place. These M_c values are representative of natural field settings. In the more extreme and possibly unrealistic case of $M_c = 1.2$, salt was quickly swept out of the source boundary layer, flushed toward the downstream end and then out of the extended domain; therefore no slipstream was detected beneath the boundary layer when the solute was reloaded into the system.

[47] Similar qualitative trends in the previously described diagnostics were found for mixed convection cases, provided that $M_c \gg 1$ (i.e., free convection is still very important). The magnitude of the diagnostics differs because of changes in overall salt balance of model domain (e.g., TM, COG) when this open system is considered.

[48] Note that in 2-D, fingers and blobs are forced to the downstream boundary as the regional flow cannot go around the fingers in the third dimension. This has the effect of diminishing or killing free convective fingers. In any real 3-D groundwater system, advection of regional groundwater may bypass vertically descending fingers, and hence, density driven fingering is expected to be stronger in a 3-D system than in a 2-D counterpart [e.g., *Zimmermann et al.*, 2006]. These dimensionality effects on mixed convection processes warrant further examination.

4. Summary and Conclusions

[49] This numerical simulation study has clearly shown that solute transport processes associated with free convection can be significantly impacted by transient periodic solute loading using solute-on-solute-off sequences of equal duration. Important and previously undocumented phenomena (i.e., the free convection slipstream which leads to a boundary layer convective memory when the period of the solute loading is less than the critical transitional convective periodicity) were observed and analyzed. Numerical simulations were quantified by a series of objective measureable characteristics in addition to qualitative visual inspection. A set of mixed convection cases was also simulated in order to examine plume behavior in more natural settings.

[50] We conclude our study with the following remarks.

[51] 1. A modified Elder problem was developed from the classic Elder problem by making several changes. We adopted dispersive parameters (i.e., isotropic dispersivities 1.0 m; diffusion coefficient 2.8×10^{-9} m^2/s) that are representative of solute transport problems to replace the large diffusion value (i.e., 3.565×10^{-6} m^2/s) more appropriate for heat transfer problems [*Elder*, 1967] but which is still routinely used in the classic Elder problem [*Voss and Souza*, 1987]. The zero bottom concentration boundary condition was changed to no solute flux, for it is unlikely to occur and discharge salt in natural settings. The density of intruding solute (i.e., 1200 kg/m^3) was still preserved as this density is typical of a salt lake problem with high concentration. Recognizing the link between the density difference employed in the classic Elder problem and its natural equivalence in groundwater hydrology has not been made in previous literature. Modifications employed in this paper caused *Ra* of the classic Elder problem to increase from 400 to about 2×10^6, indicating a much more unstable system which can develop many fingers in the region.

[52] 2. Periodic solute loading was imposed by constant concentration along the top source boundary with equal duration of T_{on} and T_{off} periods. Plume fingers were produced during T_{on} but were not during T_{off}. In the solute off periods, existing fingers had the potential to become detached from the top source boundary. Results clearly demonstrate that the constant solute loading case maximizes the total solute transport compared with periodic solute loading functions and that solute loading periodicity is a key parameter affecting the fingering process and total solute transport behavior. Transient solute loading is more important in unstable free convection than has previously been recognized.

[53] 3. A free convection slipstream (i.e., the downward movement of groundwater associated with a convection cell behind a descending salt blob) has been observed such that newly developed successor fingers are drawn toward the tails of convection cells associated with predecessor fingers.

[54] 4. The free convection slipstream may intersect the source boundary condition layer, creating a boundary layer convective memory, when the periodicity of the solute loading is smaller than a critical transitional convective periodicity (approximately 5 to 10 years T_{on} time for the current setting). This is the minimum time scale that produces complete disconnection of saline fingers from the source boundary and where successor and predecessor fingers sets become mutually exclusive for larger periods. Periodicity smaller than the critical transitional convective periodicity leads to an important enhanced mechanism for solute transport. The comparison of TM demonstrates that the boundary layer convective memory causes the total mass transferred through the top boundary to be considerably larger when the period of solute cycling is much smaller (i.e., from $T_{0.5}$ to $T_{0.1}$) than the critical transitional convective periodicity.

[55] 5. The boundary layer convective memory may cause new fingers to form in the same locations and migrate in same pathways as their predecessor fingers. These newly developed successor fingers will reinforce their predecessor fingers and lead to enhanced solute transport. In these cases predecessor and successor sets of fingers are mutually dependent.

[56] 6. The macroscopic and microscopic diagnostics quantify the existence of the free convection slipstream, boundary layer convective memory, and critical transitional convective periodicity. *Sh* in every cyclic loading case spikes to a very high value at the start of each period of solute cycling but quickly decreases to a common range during T_{on}; *Sh* is gradually weakened by the accumulating salt. COG ascends during T_{on} and descends during T_{off}, but asymptotes to the vertical center of the domain as the aquifer fills with solute. NOF of cyclic loading cases is maintained at a quantity close to that of the constant loading case during T_{on}, but decreases with increasing period of solute cycling during T_{off}. The behavior of accumulating salt promotes the decrease in 0.2 NOB and the increase in 0.6 NOB. Macroscopic diagnostics (*Sh*, TM, and COG) exhibit smaller variability

than microscopic ones (NOF and NOB) due to their spatial and temporal integral characteristics. In the case of TM, only a factor of two variability was observed for all periodicity cases, and this was significantly smaller than the variability amongst cases when considering microscopic diagnostics. These results clearly suggest better prediction of solute transport behavior may be expected when using macroscopic rather than microscopic diagnostics.

[57] 7. In the case of mixed convection, salt entering through the top source boundary is compelled to move to the downstream boundary, and the strength of advective movement increases as the characteristic mixed convection ratio (M_c) is reduced. The slipstream phenomenon is still seen to occur in cases of moderate to large M_c, especially in the case of $M_c = 120$, which may be representative of salt lakes having high salinity difference between overlying dense water and groundwater and more reasonable advection encountered in a field case. As the strength of advection increases and the mixed convection ratio is significantly reduced, the old predecessor plume may be swept away from the boundary layer entirely in the solute loading-off period. In these strongly advective cases, there is little or no opportunity for a boundary layer convective memory to develop, irrespective of the periodicity of the solute loading. The strongly advective case considered in this study, which resulted in the entire predecessor plume being swept from the boundary, employed an artificially large hydraulic head gradient.

[58] This study has systematically examined the role of transient solute loading on free convection in porous media. To the best of our knowledge, the phenomena of a boundary layer convective memory associated with a free convection slipstream and their important relationship with a critical transitional convective periodicity have not been reported in previous literature. Results clearly show that the inclusion of periodic solute loading leads to entirely different solute transport dynamics when compared with the case of the constant source boundary condition. Periodicity also affects the total amount of solute involved in the transport process. Where a constant concentration boundary condition is employed as an approximation for the transient case, it provides a conservative overestimate of the total solute entering the region. Transient solute loading is clearly more important in unstable free convection in porous media than has previously been recognized or documented.

[59] Further work is required to evaluate plume behavior under transient solute loading conditions which are more representative of natural variations (e.g., sinusoidal changes, complex time series data for the salinity source). It will also be useful to compare results for solute and thermal systems. Laboratory and/or field experiments should be considered to verify the physical existence of these transient phenomena. Finally, the importance of spatial geologic heterogeneity in free convection phenomena has recently been documented in a number of studies. A systematic comparison of the relative strengths of spatial and temporal heterogeneity within a unified framework would constitute a useful future analysis. Similarly, the influence of transient solute loading on the applicability of an average Rayleigh number (based on mean time-averaged quantities) for predicting the onset of convection in porous media warrants exploration.

[60] **Acknowledgments.** The authors gratefully acknowledge Hans Diersch for helpful advice on the use of the FEFLOW software. Author Y. Xie wishes to acknowledge the financial support provided by a CSC living stipend scholarship of the Chinese government, a fee waiver scholarship of Flinders University of South Australia, and a scholarship by the National Centre for Groundwater Research and Training for the postgraduate study. This work was funded by the National Centre for Groundwater Research and Training, a collaborative initiative of the Australian Research Council and the National Water Commission.

References

Abarca, E., J. Carrera, X. Sánchez-Vila, and M. Dentz (2007), Anisotropic dispersive Henry problem, *Adv. Water Resour.*, *30*, 913–926.

Ackerer, P., A. Younes, and R. Mose (1999), Modeling variable density flow and solute transport in porous medium: 1. Numerical model and verification, *Transp. Porous Media*, *35*(3), 345–373.

Adams, J. J., and S. Bachu (2002), Equations of state for basin geofluids: Algorithm review and intercomparison for brines, *Geofluids*, *2*, 257–271.

Bear, J. (1972), *Dynamics of Fluids in Porous Media*, Elsevier, New York.

Butler, G. P. (1969), Modern evaporite deposition and geochemistry of coexisting brines, the Sabkha, Trucial coast, Arabian gulf, *J. Sediment. Petrol.*, *39*(1), 70–89.

Chhuon, B., and J. P. Caltagirone (1979), Stability of a horizontal porous layer with timewise periodic boundary conditions, *J. Heat Transfer*, *101*(2), 244–248.

Diersch, H. J. G. (2005), FEFLOW: Finite Element Subsurface Flow & Transport Simulation System, software, WASY GmbH Inst. for Water Resour. Plann. and Syst. Res., Berlin.

Diersch, H. J. G., and O. Kolditz (2002), Variable-density flow and transport in porous media: Approaches and challenges, *Adv. Water Resour.*, *25*, 899–944.

Elder, J. W. (1967), Transient convection in a porous medium, *J. Fluid Mech.*, *27*(3), 609–623.

Fan, Y., C. J. Duffy, and D. S. Oliver (1997), Density-driven groundwater flow in closed desert basins: Field investigations and numerical experiments, *J. Hydrol.*, *196*, 139–184.

Frind, E. O. (1982), Simulation of long-term transient density-dependent transport in groundwater, *Adv. Water Resour.*, *5*, 73–88.

Graf, T., and R. Therrien (2007), Variable-density groundwater flow and solute transport in irregular 2D fracture networks, *Adv. Water Resour.*, *30*, 455–468.

Gresho, P. M., and R. L. Lee (1981), Don't suppress the wiggles—They're telling you something!, *Comput. Fluids*, *9*, 223–253.

Horton, C. W., and F. T. Rogers (1945), Convection currents in a porous medium, *J. Appl. Phys.*, *16*, 367–370.

Kolditz, O., R. Ratke, H. J. G. Diersch, and W. Zielke (1998), Coupled groundwater flow and transport: 1. Verification of variable-density flow and transport models, *Adv. Water Resour.*, *21*, 27–46.

Kooi, H., J. Groen, and A. Leijnse (2000), Modes of seawater intrusion during transgressions, *Water Resour. Res.*, *36*(12), 3581–3589.

Lapwood, E. R. (1948), Convection of a fluid in porous medium, *Math. Proc. Cambridge Philos. Soc.*, *44*, 508–521.

Lenkopane, M., A. D. Werner, D. A. Lockington, and L. Li (2009), Influence of variable salinity conditions in a tidal creek on riparian groundwater flow and salinity dynamics, *J. Hydrol.*, *375*, 536–545.

Mazzia, A., L. Bergamaschi, and M. Putti (2001), On the reliability of numerical solutions of brine transport in groundwater: analysis of infiltration from a salt lake, *Transp. Porous Media*, *43*(1), 65–86.

Nield, D. A., and A. Bejan (2006), *Convection in Porous Media*, 3rd ed., Springer, Berlin.

Oldenburg, C. M., and K. Pruess (1995), Dispersive transport dynamics in a strongly coupled groundwater-brine flow system, *Water Resour. Res.*, *31*(2), 289–302.

Post, V. E. A., and H. Prommer (2007), Multicomponent reactive transport simulation of the Elder problem: Effects of chemical reactions on salt plume development, *Water Resour. Res.*, *43*, W10404, doi:10.1029/2006WR005630.

Prasad, A., and C. T. Simmons (2003), Unstable density-driven flow in heterogeneous porous media: A stochastic study of the *Elder* [1967b] "short heater" problem, *Water Resour. Res.*, *39*(1), 1007, doi:10.1029/2002WR001290.

Prasad, A., and C. T. Simmons (2005), Using quantitative indicators to evaluate results from variable-density groundwater flow models, *Hydrogeol. J.*, *13*, 905–914.

Riaz, A., M. Hesse, H. A. Tchelepi, and F. M. Orr Jr. (2006), Onset of convection in a gravitationally unstable diffusive boundary layer in porous media, *J. Fluid Mech.*, *548*, 87–111.

Schincariol, R. A., and F. W. Schwartz (1990), An experimental investigation of variable density flow and mixing in homogeneous and heterogeneous media, *Water Resour. Res.*, *26*(10), 2317–2329.

Schulze-Makuch, D. (2005), Longitudinal dispersivity data and implications for scaling behavior, *Ground Water*, *43*(3), 443–456.

Simmons, C. T. (2005), Variable density groundwater flow: From current challenges to future possibilities, *Hydrogeol. J.*, *13*, 116–119.

Simmons, C. T., and K. A. Narayan (1997), Mixed convection processes below a saline disposal basin, *J. Hydrol.*, *194*, 263–285.

Simmons, C. T., K. A. Narayan, and R. A. Wooding (1999), On a test case for density-dependent groundwater flow and solute transport models: The salt lake problem, *Water Resour. Res.*, *35*(12), 3607–3620.

Simmons, C. T., T. R. Fenstemaker, and J. M. Sharp Jr. (2001), Variable-density groundwater flow and solute transport in heterogeneous porous media: Approaches, resolutions and future challenges, *J. Contam. Hydrol.*, *52*, 245–275.

Van Dam, R. L., C. T. Simmons, D. W. Hyndman, and W. W. Wood (2009), Natural free convection in porous media: First field documentation in groundwater, *Geophys. Res. Lett.*, *36*, L11403, doi:10.1029/2008GL036906.

van Reeuwijk, M., S. A. Mathias, C. T. Simmons, and J. D. Ward (2009), Insights from a pseudospectral approach to the Elder problem, *Water Resour. Res.*, *45*, W04416, doi:10.1029/2008WR007421.

Voss, C. I., and W. R. Souza (1987), Variable density flow and solute transport simulation of regional aquifers containing a narrow freshwater-saltwater transition zone, *Water Resour. Res.*, *23*(10), 1851–1866.

Wood, W. W., W. E. Sanford, and A. R. S. Al Habshi (2002), Source of solutes to the coastal sabkha of Abu Dhabi, *Geol. Soc. Am. Bull.*, *114*(3), 259–268.

Wooding, R. A., S. W. Tyler, and I. White (1997), Convection in groundwater below an evaporating salt lake: 1. Onset of instability, *Water Resour. Res.*, *33*(6), 1199–1217.

Zhang, H., and F. W. Schwartz (1995), Multispecies contaminant plumes in variable density flow systems, *Water Resour. Res.*, *31*(4), 837–847.

Zimmermann, S., P. Bauer, R. Held, W. Kinzelbach, and J. H. Walther (2006), Salt transport on islands in the Okavango Delta: Numerical investigations, *Adv. Water Resour.*, *29*, 11–29.

C. T. Simmons, A. D. Werner, and Y. Xie, National Centre for Groundwater Research and Training, Flinders University, GPO Box 2100, Adelaide, SA 5001, Australia. (craig.simmons@flinders.edu.au)

J. D. Ward, SA Water Centre for Water Management and Reuse, University of South Australia, GPO Box 2471, Adelaide, SA 5001, Australia.